MIT Open Access Articles

Laboratory Observation of Localized Onset of Magnetic Reconnection

Massachusetts Institute of Technology

Laboratory Observation of Localized Onset of Magnetic Reconnection

Noam Katz,* Jan Egedal, Will Fox, Ari Le, Jeff Bonde, and Arturs Vrublevskis

*Department of Physics/Plasma Science and Fusion Center, Massachusetts Institute of Technology,
Cambridge, Massachusetts 02139, USA*

Magnetic reconnection is a fundamental process in plasmas that results in the often explosive release of stored magnetic energy, but the trigger for its onset is not well understood. We explore this trigger for fast reconnection in toroidal experiments using a magnetic x-type geometry in the strong guide-field regime. We find that the onset occurs asymmetrically: the reconnection begins on one side of the torus and propagates around approximately at the Alfvén speed. The fast reconnection occurs only in the presence of a global plasma mode, which breaks the axisymmetry and enables the current at the x line to decrease sharply. A simple semiempirical model is used to describe the onset's growth rate.

Magnetic reconnection [1] is the often explosive release of magnetically stored energy in the presence of a plasma. This phenomenon, which involves a change in magnetic-field topology, is thought to occur, for example, in solar flares [2], magnetospheric substorms [3], and tokamak sawteeth [4]. There has been much progress in 2D, steady-state reconnection [5], but the time-dependent problem—necessary to account for explosive reconnection—and the properties of reconnection in 3D are not well understood.

In order for explosive energy release to occur, there must be a period of slow accumulation of magnetic energy, followed by a sudden transition to fast reconnection. This transition—the so-called "trigger problem"—has been explored in 2D both analytically [6–8] and numerically [9,10] using ideas including nonlinear mode excitation and bistable numerical solutions.

Meanwhile, recent measurements in tokamaks [11,12] have shown that sawtooth onset is localized both toroidally and poloidally and that the temperature profile flattening is well organized as opposed to stochastic. These 3D effects in reconnection onset appear even though the applied magnetic-field geometry is mainly 2D. In less-constrained experiments of spheromak merging, 3D reconnection structures were observed, which resulted in very strong ion heating [13]. In addition, observations of reconnection on the Sun have indicated the presence of strong 3D effects [14]. Despite the improved measurement techniques applied in tokamaks and solar observations, the internal magnetic and electrical 3D structure of the reconnection region is largely unknown.

In this Letter we describe observations of the localized (3D) onset of magnetic reconnection in a well-diagnosed laboratory experiment. After the onset, the reconnection spreads toroidally to the rest of the device, suggestive of recent observations of solar flares [15]. The reconnection is only observed when the magnetic geometry permits a global mode structure outside the reconnection region. We discuss the implications of the onset for current con-

tinuity, provide a simple semiempirical model for the gross features of the onset, and describe the interchangelike character of the global mode.

The experiments were conducted on the Versatile Toroidal Facility (VTF) at MIT with a setup similar to [16], and are shown in Fig. 1(a). An inductive current is driven toroidally in the argon plasma to build up its density ($\sim 2 \times 10^{18}$ m^{-3}) and temperature ($T_e \sim 15$ eV, but $T_i \sim 1$ eV) and drive toroidal current in four internal coils. The resulting magnetic configuration in the poloidal cross section includes the familiar x-line geometry. The dominant magnetic field, however, is the toroidal field ($B_\varphi = B_0 R_0 / R$, $B_0 = 56$ mT, $R_0 = 1$ m). The plasma is diagnosed by multiple arrays of Rogowski coils and magnetic and Langmuir probes.

To initiate reconnection, we redistribute the currents in the four internal coils in such a way as to build up the toroidal current at the x line (by Lenz's law). The internal
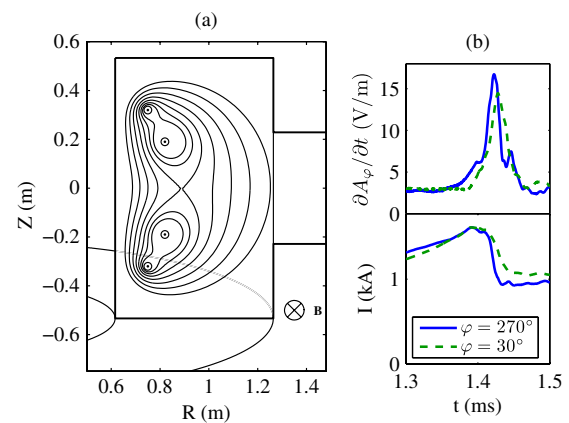

FIG. 1 (color online).   (a) Schematic of VTF chamber showing the four internal coils and in-plane projections of the magnetic-field lines. (b) Reconnection rate ($\partial A_\varphi / \partial t$) and current near the x line vs time at two toroidal angles; reconnection is not simultaneous. The currents have been normalized to the same peak value to more clearly show the time delay.

coil currents are up-down symmetric. In some discharges, after a delay of 100 μs the x-line current decreases suddenly [16]. This spontaneous decrease in current [Fig. 1(b)] is accompanied by a spike in the toroidal inductive electric field, which we take as the reconnection rate. Just before the spontaneous reconnection, the width of the current channel approaches ρ_s, the ion-sound gyro-radius. As a result of the reconnection, a significant portion of the magnetic energy released drives Alfvénic plasma outflows, and electron heating is also observed [16]. However, as Fig. 1(b) shows, the plasma response is not toroidally symmetric.

Thus, although the experimental setup is symmetric, we find here that the reconnection onset is toroidally localized. Figure 2 shows the reconnection rate ($-\partial A_\varphi/\partial t$) at various times (top row), viewed from above. The reconnection starts at one toroidal location, and then propagates in both directions around the torus. The propagation speed is approximately twice the Alfvén speed, although on this time scale the ions are only marginally magnetized. While asymmetries in the in-vessel coils may influence the onset angle, this angle does vary among different discharges. Here we take the onset angle to be 270°, which is the most frequent location. We compute $\partial A_\varphi/\partial t$ in Fig. 2 as $(1/R) \int \dot{B}_z R dR$ from $\dot{B}_z$ measurements, a method appli-

cable for this experiment, which has a strong guide magnetic field [17].

In the second row of Fig. 2, the toroidal electrostatic field evaluated at the x line (ϕ_x) is added to $\partial A_\varphi/\partial t$. Note that we split the potential $\phi = \phi_x(\varphi) + \phi_{\text{in-plane}}(\mathbf{r})$, where ϕ_x is poloidally uniform. We see that the total electric field remains toroidally localized and is enhanced at the onset location ($\varphi = 270°$); the enhancement may be surprising, but it is related to a global mode away from the x line. The third row shows $\phi_{\text{in-plane}}$ at $\varphi = 270°$. We approximate the in-plane plasma potential by the floating potential, since it is unlikely that temperature variations produce the strong (60 V) structure in the floating potential, and the measured I-V response of Langmuir probes is well described with Maxwellian electrons. Also shown are cross sections of the toroidal current density at two different toroidal angles. The first row of current density was measured near the onset location; superimposed on it are magnetic-field lines projected onto the plane, measured by a novel flux probe array [17]. The second row is at a different toroidal location; the current density is clearly not toroidally symmetric.

Further evidence of the asymmetry is seen in the electrostatic potential measurements, shown in Fig. 3 at one time slice. A global 3D mode arises in conjunction with fast
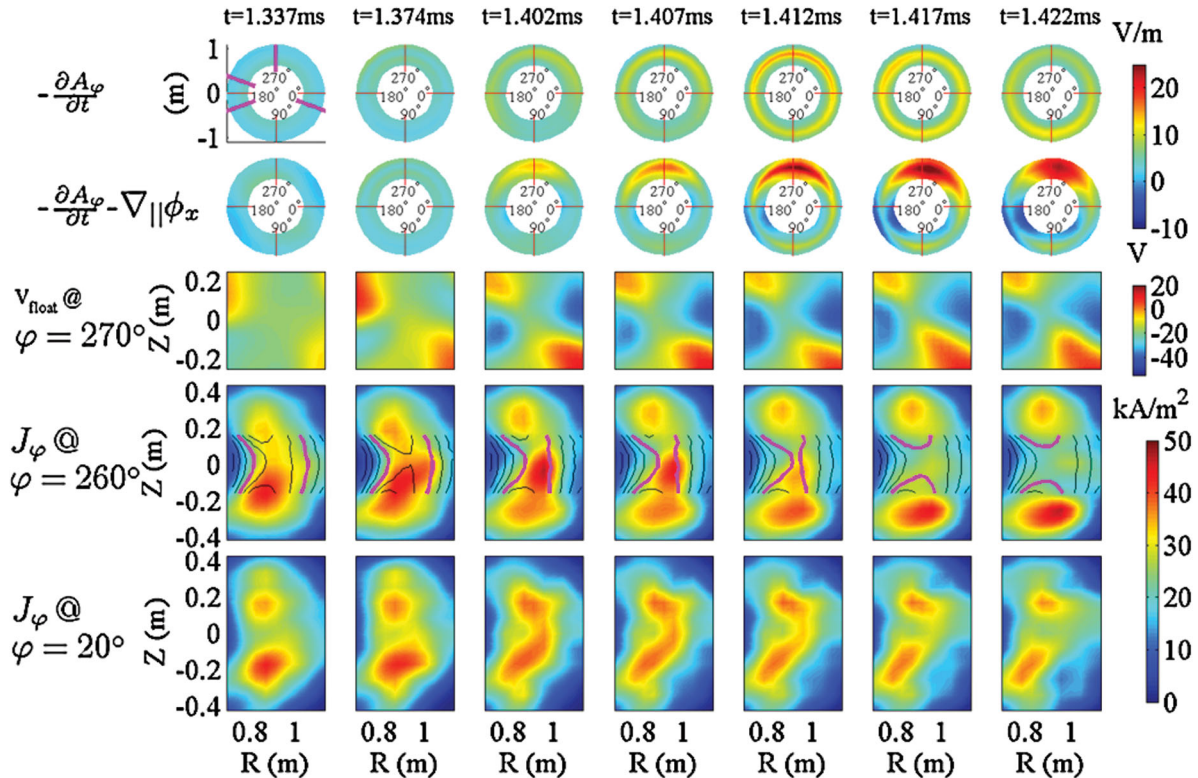

FIG. 2 (color).   The 3D measurements of magnetic reconnection on VTF at various times. Row 1: inductive electric field propagating around the device (measured at six toroidal locations); reconnection peaks at $t = 1.412$ ms. Row 2: toroidal electric field, which includes the electrostatic component, remains toroidally localized. Row 3: floating potential measured near onset and growing in time. Rows 4–5: toroidal current density (at 8 cm resolution) at two cross sections ($\varphi = 20°$, 260°), with overlaid poloidal magnetic-field lines. The stressed angle of the x line shows a strong departure from the 90° of a vacuum x line. The current, which does not include the in-vessel coil current, is clearly toroidally asymmetric.
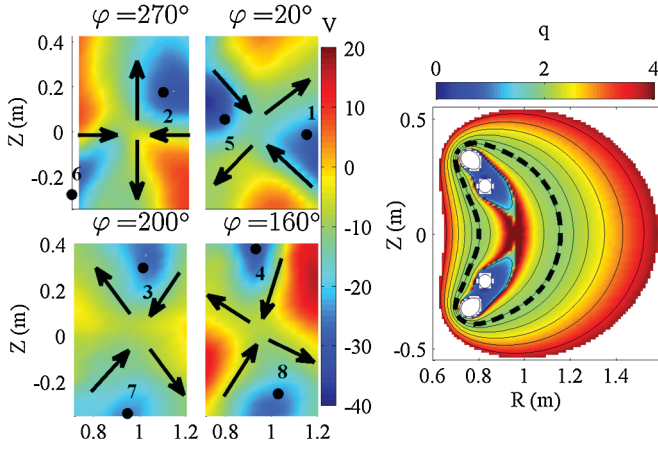
FIG. 3 (color). Left panels: floating potential measured at $t = 1.412$ ms, at the four cross sections indicated in the top row of Fig. 2. Black arrows represent $\mathbf{E} \times \mathbf{B}$ velocity. Right panel: $q \simeq 2$ over a large part of the cross section. The $q \simeq 2$ rotation of the field-aligned potential is evident from the highlighted dashed field line whose sequential puncture points are shown on the left panels in black. The rationality of q is required for the potential to map onto itself.

reconnection, and its amplitude increases in time with the reconnection rate. In a previous experiment with toroidal symmetry [18], a quadrupolar axisymmetric potential was found to arise naturally to maintain $\mathbf{E} \cdot \mathbf{B} = E_\varphi B_\varphi + \mathbf{B} \cdot \nabla \phi_{\text{in-plane}} = 0$ when ~ 5 cm away from the x line. That potential was very similar to the one in Fig. 3 measured at the reconnection onset location ($\varphi = 270°$). Thus, here too, ϕ develops to cancel the $E_\varphi B_\varphi$ portion of $\mathbf{E} \cdot \mathbf{B}$ in the region where $q \simeq 2$. When toroidally away from the onset location, the potential structure rotates with the magnetic-field lines, breaking axisymmetry.

The field line rotation can be described using the tokamak safety factor q, the number of times a field line goes around toroidally for one poloidal circuit. We find that fast reconnection is only observed for rational q, specifically when $q \simeq 2$ or $q \simeq 3$ outside the x-line region (Fig. 3). When q is rational, the magnetic-field lines close on themselves after only a few toroidal circuits. Rational q is required for the potential of the mode to develop. In this Letter, only the $q = 2$ case is discussed.

The rotating potential is associated with interchange-type motion: where q is rational and roughly uniform, flux tubes of plasma can move without bending the magnetic field. This poloidal $\mathbf{E} \times \mathbf{B}$ motion is given by $\nabla \phi_{\text{in-plane}} \times \hat{\mathbf{e}}_\varphi / B_\varphi$ and it is shown schematically by the arrows in Fig. 3.

The potential structure of Fig. 3 is essential for explaining current continuity. Asymmetric reconnection implies that the field-aligned current at the x line no longer closes in toroidal loops. From $A_\varphi = \mu_0/(4\pi) \int (J_\parallel/|\mathbf{r}' - \mathbf{r}|)d^3\mathbf{r}'$, it follows that a local increase in $-\partial A_\varphi/\partial t$ must be associated with a local decrease in the parallel current density. Since $\nabla_\parallel J_\parallel + \nabla_\perp \cdot \mathbf{J}_\perp = 0$, there must be perpendicular

currents that compensate for the asymmetry. In our case, these are ion polarization currents, controlled by the potential of Fig. 3. The analysis in Ref. [19] shows that the ions are sufficiently magnetized that $J_\perp = (mn/B^2)d\nabla_\perp \phi/dt$, and we can write the asymmetric part of the parallel current as

$$J_\parallel(\mathbf{r}) = J_{\text{edge}} + \int_{\text{edge}}^{\mathbf{r}} \frac{mn}{B^2} \nabla_\perp^2 \frac{\partial \phi}{\partial t} dl, \qquad (1)$$

where the integral is evaluated along field lines with n uniform, and the nonlinear part of the time derivative was dropped ($d/dt \rightarrow \partial/\partial t$). J_{edge} is assumed to be evenly distributed at the two edges of each field line.

To evaluate Eq. (1) we use model fields chosen to match the experiment. The magnetic field near the x line is approximated by

$$\mathbf{B} = b_0(z\hat{\mathbf{r}}/\alpha + \alpha r\hat{\mathbf{z}} + l_0\hat{\boldsymbol{\varphi}}), \qquad (2)$$

where $b_0 = 0.035$ T/m, $l_0 = 1.7$ m, and $\alpha = 1.7$ (to reflect finite current density); α is assumed to be toroidally uniform since we focus only on the early, linear stage. The rotating potential ($\phi_{\text{in-plane}}$) is approximated by

$$\begin{aligned}
\phi &= \phi_0 \log\left[\frac{z'^2 + \delta^2}{r'^2 + \delta^2}\right], \\
r' &= \cos(\Delta\varphi/2)r\sqrt{\alpha} + \sin(\Delta\varphi/2)z/\sqrt{\alpha}, \\
z' &= -\sin(\Delta\varphi/2)r\sqrt{\alpha} + \cos(\Delta\varphi/2)z/\sqrt{\alpha},
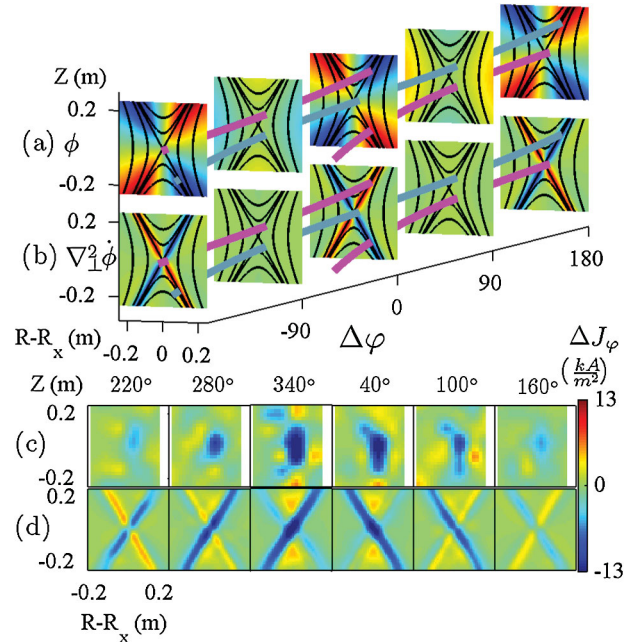\end{aligned} \qquad (3)$$

FIG. 4 (color). (a) Potential model [Eq. (3)] with the gray magnetic-field line, which passes by the x line near the onset location ($\Delta\varphi = 0$); (b) divergence of ion polarization currents $\propto \nabla_\perp^2 \dot\phi$; (c) experimentally measured change in J_φ during 8 μs leading up to peak reconnection; (d) integration of (b) along field lines [Eq. (1)], which gives an asymmetric parallel current.
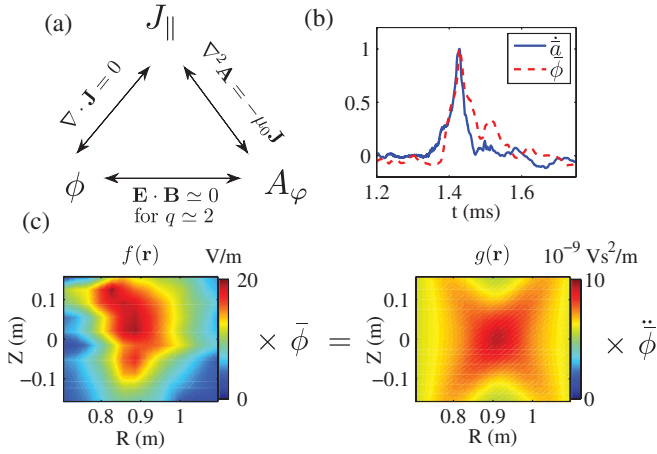
FIG. 5 (color). (a) Schematic representation of the model for the reconnection's onset; (b) mode amplitude (max-min) and peak reconnection rate vs time; (c) Eq. (5) shown graphically.

where $\Delta\varphi = \varphi - \varphi_{\text{onset}}$, and $\delta = \delta_0[1 - \frac{2}{3}\cos(2\Delta\varphi)]$, $\phi_0 = 6$ V, and $\delta_0 = 0.12$ m are found from fitting Eq. (3) to the experimentally measured potential. We then calculate the ion polarization currents associated with this potential growing in time [Fig. 4(b)] and integrate along field lines using Eq. (1). The result for the asymmetric toroidal current is shown in Fig. 4(d); it is consistent with a toroidally localized decrease in $J_\parallel$ at the x line, with magnitude similar to that of the experimental data [Fig. 4(c)]. The disagreement along the separatrix may be due to the assumptions of uniform density, linear geometry, or the simplified potential model. Alternatively, it is possible that slight magnetic stochasticity affects the separatrix specifically because of its long integration paths in Eq. (1). Nevertheless, the key to the toroidal localization is the rotating potential: two field lines near the x line at $\Delta\varphi = 0°$ and $180°$ (Fig. 4, gray and magenta, respectively) sample different potentials because of the asymmetry. Therefore, their contributions to $J_\parallel$ are opposite.

We can use Eq. (1) with a few other observations to model the main features of the 3D reconnection onset. We focus only on the first 10–20 μs, i.e., before the inductive electric field propagates around the torus. A cartoon of the model is shown in Fig. 5(a). We use the connection between A_φ and $J_\parallel$, the fact that $J_\parallel$ and ϕ are related by current continuity, and an empirical Ohm's law to relate A_φ and ϕ. A combination of these relations gives an exponentially growing reconnection rate.

To demonstrate this, we write A_φ using Eq. (1):

$$A_\varphi \simeq \frac{\mu_0}{4\pi} \int \left(\int \frac{mn}{B^2} \nabla_\perp^2 \dot{\phi} \, dl \right) \frac{d^3\mathbf{r}'}{|\mathbf{r}' - \mathbf{r}|}. \quad (4)$$

Next we use the empirical observation that the inductive electric field and the mode amplitude grow in time together. More precisely, we assume that $\partial A_\varphi(\mathbf{r}, t)/\partial t = \tilde{A}(\mathbf{r})\dot{a}(t)$ and $\phi(\mathbf{r}, t) = \tilde{\Phi}(\mathbf{r})\bar{\phi}(t)$, where $\dot{a}$ and $\bar{\phi}$ vary

between 0 and 1, and, for each time point, $\dot{a}$ is computed as a spatial average near the x line and $\bar{\phi}$ is computed as the rms value. The empirical observation is then $\dot{\bar{a}} = \bar{\phi}$ [see Fig. 5(b)], and we rewrite Eq. (4) as

$$\tilde{A}\,\bar{\phi} \simeq \left[\frac{\mu_0}{4\pi} \int \left(\int^{\mathbf{r}'} \frac{mn}{B^2} \nabla_\perp^2 \tilde{\Phi} dl \right) \frac{d^3\mathbf{r}'}{|\mathbf{r}' - \mathbf{r}|} \right]\ddot{\bar{\phi}}. \quad (5)$$

This equation has the form $f(\mathbf{r})\bar{\phi}(t) = g(\mathbf{r})\ddot{\bar{\phi}}(t)$, which—if $f(\mathbf{r}) \propto g(\mathbf{r})$ and $f/g > 0$—gives exponential growth for ϕ. We use the experimentally measured value for $\tilde{A}$ and use Eqs. (2) and (3) for B and $\tilde{\Phi}$ to compute the integral for $g(\mathbf{r})$. Figure 5(c) represents Eq. (5) graphically and shows that, indeed, $f(\mathbf{r})$ and $g(\mathbf{r})$ have similar forms. Then we set $\bar{\phi} = \exp(\gamma t)$ to find a growth rate of $(22\ \mu\text{s})^{-1}$, which agrees well with the experimental value of $(20 \pm 6\ \mu\text{s})^{-1}$, found from exponential fitting of $\dot{\bar{a}}$ in Fig. 5(b); the uncertainty represents the standard deviation of the growth rates in many discharges.

A very similar analysis was carried out in Ref. [18] for toroidally symmetric reconnection. In that experiment, Eq. (1) gave an enhancement in $J_\parallel$ at the x line, which caused an oscillatory solution $\phi \sim \sin\omega t$. In 3D, the situation is fundamentally different: due to the 3D effects, the increasing ϕ causes a local decrease in $J_\parallel$. This reversal in sign enables the exponentially growing solution $\phi \sim \exp(\gamma t)$ that we observe.

*nkatz@mit.edu
[1] J. Dungey, Phys. Rev. Lett. **6**, 47 (1961)
[2] M. Aschwanden, *Physics of the Solar Corona: An Introduction* (Praxis Publishing, Chichester, UK, 2004)
[3] A. T. Y. Lui, J. Geophys. Res. **101**, 13067 (1996).
[4] S. von Goeler et al., Phys. Rev. Lett. **33**, 1201 (1974).
[5] M. Yamada, Phys. Plasmas **14**, 058102 (2007).
[6] F. L. Waelbroeck, Phys. Rev. Lett. **70**, 3259 (1993).
[7] A. Lichtenberg et al., Nucl. Fusion **32**, 495 (1992).
[8] X. Wang and A. Bhattacharjee, Phys. Rev. Lett. **70**, 1627 (1993).
[9] P. A. Cassak, M. A. Shay, and J. F. Drake, Phys. Rev. Lett. **95**, 235002 (2005).
[10] P. Pritchett, Phys. Plasmas **12**, 062301 (2005).
[11] H. K. Park et al., Phys. Rev. Lett. **96**, 195003 (2006).
[12] T. Munsat et al., Nucl. Fusion **47**, L31 (2007).
[13] M. R. Brown et al., Phys. Plasmas **9**, 2077 (2002).
[14] P. Démoulin et al., Astron. Astrophys. **325**, 305 (1997).
[15] L. Li et al., Astrophys. J. **690**, 347 (2009).
[16] J. Egedal et al., Phys. Rev. Lett. **98**, 015003 (2007).
[17] A. Kesich et al., Rev. Sci. Instrum. **79**, 063505 (2008).
[18] J. Egedal et al., Phys. Rev. Lett. **90**, 135003 (2003).
[19] J. Egedal et al., Phys. Plasmas **12**, 052107 (2005).